



A novel structure tube for supercritical CO₂ turbulent flow with high non-uniform heat flux

Yan Juan Wang^{a,*}, Shuo Gao^a, Wei Jie Shi^a, Qi Bin Liu^{b,c}, Jin Liang Xu^a

^a The Beijing Key Laboratory of Multiphase Flow and Heat Transfer, North China Electric Power University, Beijing 102206, China

^b Institute of Engineering Thermophysics, Chinese Academy of Sciences, Beijing 100190, China

^c University of Chinese Academy of Sciences, Beijing 100049, China

ARTICLE INFO

Article history:

Received 27 February 2023

Revised 3 May 2023

Accepted 9 May 2023

Available online 27 May 2023

Keywords:

High non-uniform heat flux

Supercritical carbon dioxide

Thermal-fluid-mechanical coupling

Novel structure tube

ABSTRACT

Supercritical CO₂ has been a promising alternative working medium in coal-fired power plants, high-temperature solar power systems, and fuel cells. In these cases, supercritical carbon dioxide is in a round tube under high temperature and pressure with high non-uniform heat flux. In this study, a novel structure tube is proposed by optimizing the coupling between circumferential heat flux and tube thickness on the heat-absorbing side to improve its comprehensive performance. A thermal-fluid-mechanical coupling model was developed. The novel structure can reduce maximum temperature and temperature difference effectively for the half-cycle uniform and non-uniform heat flux. The maximum thermal stress decreased by 23 and 29% and the maximum temperature decreased by 29.6 and 24.8 K for half-cycle uniform and non-uniform heat flux when the Eccentricity increased from 0 to 0.4. A comparison was made between the proposed structure, thin-walled tube, and traditional tube. Results showed that the performance of the proposed tube is the best. The maximum temperature decreases by approximately 55 K compared with the traditional and thin-walled tubes. The maximum equivalent stress of proposed tube is the smallest. Furthermore, the structure will improve the safety and economics of the tube.

© 2023 Elsevier Ltd. All rights reserved.

1. Introduction

Owing to their modest critical condition, higher thermal efficiency, and inertness, supercritical carbon dioxide (sCO₂) Brayton cycles have been considered promising power cycles for various heat sources such as traditional coal-fired power plant, renewable solar energy, and fuel cell [1–3]. Compared with the advanced water-steam Rankine cycle system, the net power generation efficiency of the sCO₂ power system is higher, additional, the leveled cost of electricity decreases by 1.32% [4]. From the global perspective, the sCO₂ power system is a superior candidate for next generation power conversion system. Fan et al. [5] summarized general and unique issues at multiple scales for sCO₂ power system. As solar thermal power generation adopts an sCO₂ Brayton cycle, the thermal efficiency can rise to 52–57% at approximately 823 K [6]. Water steam Rankine cycle cannot easily achieve greater thermal efficiency at this temperature [7]. The sCO₂ Brayton cycle at 773–1073 K is exactly in line with the characteristics of the working medium and operating temperature of solar tower thermal power generation [8]. The performance of sCO₂ in a tube near the critical

region has been widely investigated. In contrast, sCO₂ is applied in the field of coal-fired power plant, renewable solar energy, and fuel cell, all under high temperature and pressure far from the critical region [9]. Additionally, they exhibit high non-uniform heat flux (NUH).

Recently, sCO₂ fossil-fired power plants have gained significant attention [10,11]. The safety of cooling walls in a sCO₂ boiler is a challenging issue [12]. Compared with traditional water walls, the convective heat transfer coefficient of sCO₂ is lower [13] and the working temperature is higher [14]. Various strategies have been developed in recent years to decrease cooling wall temperatures and the non-uniformity of cooling walls' circumferential temperature. One of them is to lower the heat duty of the sCO₂ boiler. The flue gas recirculation [15] and expansion of boiler size can effectively reduce the boiler heat duty. However, larger boiler sizes adversely influence ignition, stable combustion, and peak regulation. Furthermore, a larger percentage of flue gas recirculation shortens the residence time of pulverized coal and lowers the burnout rate. A sCO₂ innovative boiler design is proposed [16] by partial expansion at the upper zone and double furnace, which shows a smoother, lower average heat duty.

Another alternative method is to optimize the coupling between heat fluxes in the furnace and cooling wall tubes. Zhou et al. [16] developed a symmetric flow pattern that controls half of the

* Corresponding author.

E-mail address: 90102184@ncepu.edu.cn (Y.J. Wang).

Nomenclature

C_p	specific heat capacity, $\text{J}\cdot\text{kg}^{-1}\cdot\text{K}^{-1}$
d	tube inner diameter, mm
D	tube outer diameter, mm
e	eccentric distance, mm
E_c	Eccentricity
E	elastic modulus, MPa
G	mass flux, $\text{kg}\cdot\text{s}^{-1}\cdot\text{m}^{-2}$
HUH	half-cycle uniform heat flux
L	tube length, m
NUH	non-uniform heat flux
P	working pressure, MPa
ΔP	pressure drop, kPa
q	heat flux, $\text{kW}\cdot\text{m}^{-2}$
r	tube inner radius, mm
R	tube outer radius, mm
R_T	thermal resistance
T	temperature, K
TDF	thermal deviation factor
ΔT	temperature difference, K
UH	uniform heat flux
Y	correction coefficient

Greek symbols

α	circumferential angle, or thermal expansion coefficient, K^{-1}
σ_{as}	maximum allowable stress, MPa
δ_m	minimum thickness, mm
λ	thermal conductivity, $\text{W}\cdot\text{m}^{-1}\cdot\text{K}^{-1}$
ξ	allowable stress correction factor
ν	poisson's ratio
ρ	density, $\text{kg}\cdot\text{m}^{-3}$
σ_{eq}	equivalent stress, MPa
σ_p	mechanical stress, MPa
σ_s	yield strength, MPa
σ_t	thermal stress, MPa
φ	view factor
$\bar{\varphi}$	average of view factor

Subscripts

ave	average
f	fluid
in	inlet
max	maximum
r, θ , l	radial, tangential, axial direction
w	tube wall
wi	inner wall of tube
wo	outer wall of tube

sCO_2 to flow from the middle region to the sides, thereby allowing the low-temperature sCO_2 to enter the region with high heat flux. Results showed that the maximum wall temperature distribution along the height direction of the boiler with the symmetric flow pattern is more uniform. Yang et al. [17] proposed the “cold sCO_2 -hot fire matching and cascaded temperature control” principle to reduce cooling wall temperature, and this optimal arrangement significantly reduced the temperature in overheated region 12–44 K. Liu et al. [15] optimized the matching relationships between the heat flux of flue gas side and working parameters of sCO_2 side to reduce the cooling wall temperatures. They [18] proposed an innovative “4-Part layout” for the heating modules, which can reduce the maximum cooling wall temperature by 18.66 K.

The third approach is strengthening the heat transfer process between tube and fluid to even NUH through the new structures

of tubes. Many modified structures have been proposed [19,20], and most of them are based on concentrated solar power systems [21]. Christian et al. [22] improved the system's thermal efficiency by manipulating the geometries of the receiver to reduce radiative heat loss. The enhanced heat transfer structures, such as triangular ribs tube, rectangular wing tube [23], and internal twisted tapes, [24] were widely investigated to reduce the maximum temperature and the temperature difference of the tube, while they caused large flow resistance. Li et al. [24] investigated three types of enhanced heat transfer structures. Compared with the basic smooth tube, the twisted tape insert tube, unilaterally dimpled tube and the unilaterally elliptic dimpled tube can reduce the maximum temperature (T_{\max}) by 42.24–68.28 °C, 43.8–61.66 °C and 55.81–77.33 °C, respectively. The dimpled tubes slightly increase the pressure drop, whereas the pressure drop of the twisted tape insert tube was about 4 times larger than that of basic tube.

Therefore, the design of heat-transfer enhancement structures must consider comprehensive factors such as pressure drop, thermal loss, thermal stress, and mechanical stress. Li et al. [25] proposed a performance recovery coefficient for thermal-hydraulic evaluation of recuperator in sCO_2 Brayton cycle. Additionally, most of the previous structural analyses have been conducted on smooth tubes due to complex configurations. A few studies have analyzed the mechanical properties of tubes thoroughly, which should be considered because of their modified structures.

In this study, unlike existing methods, we optimized the coupling between circumferential heat flux and circumferential tube thickness on the heat-absorbing side to improve its comprehensive performance. A three-dimensional (3D) conjugated model was developed to analyze the performance of novel structure. The distributions of temperature, pressure drop, and stress of cooling wall tubes were numerically obtained. The effects of heat flux distributions on heat transfer performance were discussed. A comparison was made between the proposed structure, thin-walled tube, and traditional tube. The present study can provide a guidance for the design and optimization of sCO_2 tube under high NUH in sCO_2 power systems.

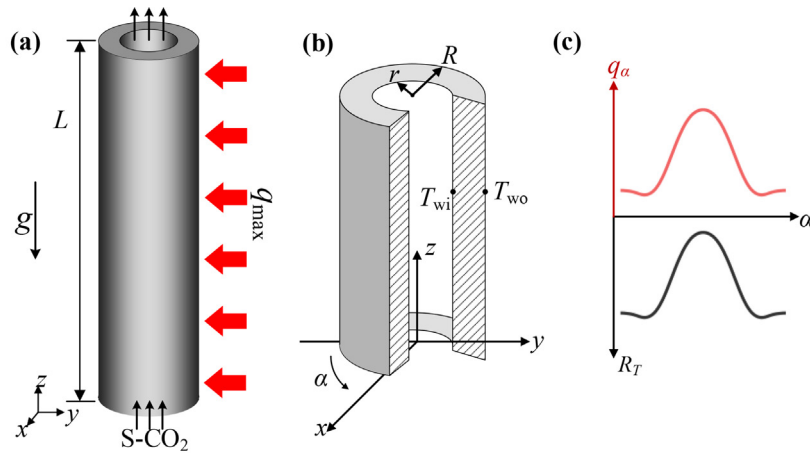
2. Numerical model and method

2.1. Traditional sCO_2 cooling wall tube

The cooling wall tube in sCO_2 coal-fired power plants was selected as the research subject to investigate the high temperature and pressure sCO_2 turbulent flow in a vertical round tube under high NUH. A tube length of 1 m, an inner radius (r) of 11 mm, and a tube thickness of 6.5 mm were considered as the basic geometric parameters (Fig. 1). It was a seamless steel tube. The sCO_2 flowed upward in the tube contrary to the gravity. The operating pressure (P) was 25 MPa, and the inlet temperature (T_{in}) was 773.15 K. The circumferential angle (α) on the bottom generatrix is defined as 0° Because of the high temperature and pressure working conditions, 316H was selected as the tube material. Its physical properties were shown in Fig. 2.

2.2. Thermal-fluid-mechanical model

A steady-state multi-physical coupling model was developed by considering the variations of sCO_2 's thermophysical properties from NIST [27]. The basic governing equations for sCO_2 flow and heat transfer in the tube include continuity, momentum, and energy equations which were described in a previous study [28–30]. We compared the calculated results with experimental data of Zhu [13], which showed that the relative errors of the k - ε model turbulence model were the smallest [10]. Thus, the k - ε turbulence model was used.



(a) Smooth tube (b) Detailed view of structure (c) Perfect matching between heat flux and circumferential heat resistance.

Fig. 1. Physical configuration of the tube.

(a) Smooth tube (b) Detailed view of structure (c) Perfect matching between heat flux and circumferential heat resistance.

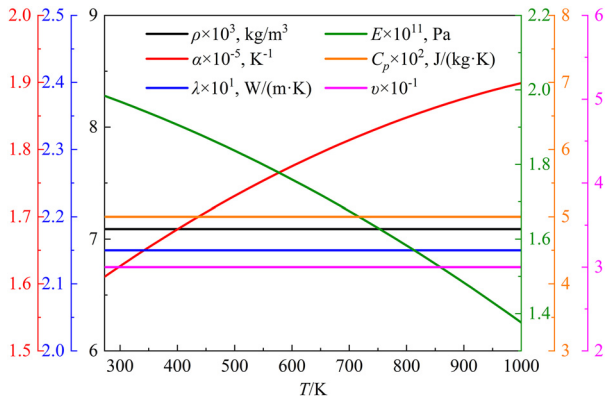


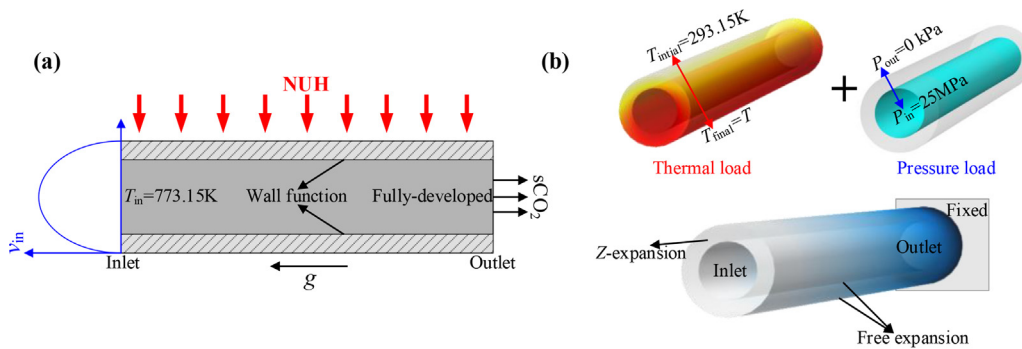
Fig. 2. Physical properties of 316H form [26].

The heat transfer pattern in the tube wall was the heat conduction. Based on the wall temperature results, the equivalent stress (σ_{eq}) and the circumferential (θ), radial (r), axial (l) thermal (σ_T) and mechanical stresses (σ_p) can be calculated by solving the cor-

responding equations [31,32]. The maximum residuals of all governing equations were below 10^{-3} .

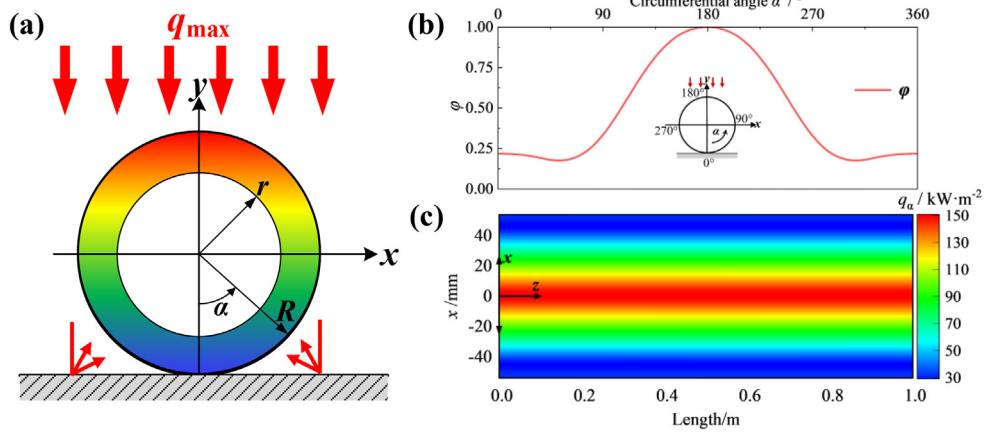
The boundary conditions for the simulation were shown in Fig. 3. It should be pointed out that in these simulations: (1) The inlet velocity was a fully developed flow velocity (a parabolic velocity profile) calculated as a function of average inlet velocity. (2) The wall function boundary condition [33] was used at the inner tube wall, a theoretical lift-off from the physical wall was assumed. (3) The outlet was set as fully-developed assumption [34]. (4) The circumferential non-uniform heat flux was used as boundary condition of outer tube surface. According to [35], radiative heat flux was only considered in the furnace calculated by the view factor ($\varphi = q_\alpha / q_{max}$) [36,37] (Fig. 4(b)). The non-uniform radiant heat flux distribution was shown in Fig. 4(c). (5) Both the thermal and pressure loads were considered in the tubes' structural analysis. As the pressure in the sCO₂ boiler was low and was assumed to be 0 kPa [38]. The stress-free reference temperature was set as 293.15 K. (6) The inlet end of the tube could expand along the flow direction only, the internal and external tube wall was free to expand and the outlet end was fixed.

The grid-independence analysis on the traditional tube was performed for the multi-physical coupling model, as shown in Fig. 5,



(a) Thermal-fluid boundary conditions (b) Structural boundary conditions

Fig. 3. Boundary conditions for the simulation. (a) Thermal-fluid boundary conditions (b) Structural boundary conditions.



(a) Cross-section irradiation profile (b) Distribution of ϕ (c) NUH distribution on a panel

Fig. 4. Non-uniform heat flux.

(a) Cross-section irradiation profile (b) Distribution of ϕ (c) NUH distribution on a panel.

Table 1
Representative experimental cases for validation.

Parameter	$G, \text{kg}/(\text{m}^2\text{s})$	L, m	T_{in}, K	$q_w, \text{kW}/\text{m}^2$	P, MPa	d, mm	D, mm	Material
Value	1250.9	2	307.4	375.03	21.014	10	12	1Cr18Ni9Ti

and the relative error of the maximum equivalent stress in the tube is < 0.01 .

2.3. Model validations

The proposed thermal-fluid model of cooling wall tube was verified by the experimental data of Zhu et al. [13] under the same working conditions as shown in Table 1. As shown in Fig. 6, the numerical results on the fluid temperature agree well with the experimental data. The relative errors of the inner tube wall temperatures are within 1.9%.

The structural model is validated by theoretical solutions, as limited experimental data are available on stress distribution in high NUH. The pressure load and temperature difference between the inner and outer surfaces were 25 MPa and 35.1 K. The distribution of the equivalent stress along the radial direction is shown in Fig. 7, which shows that the equivalent stress obtained from the

numerical calculations and theoretical analysis are consistent, confirming the accuracy of the proposed model.

3. Results and discussions

3.1. Effect of heat flux distribution

A numerical study was performed to better understand the behavior of a traditional tube under high NUH distribution, and the computational conditions were as follows: sCO_2 inlet mass flux (G) of $2000 \text{ kg}/(\text{m}^2\text{s})$, the sCO_2 inlet temperature of 773.15 K , and working pressure of 25 MPa . Three cases are selected with different heat flux distributions, as shown in Fig. 8. Cases (a) and (b) are common experimental conditions, whereas case (c) represents ac-

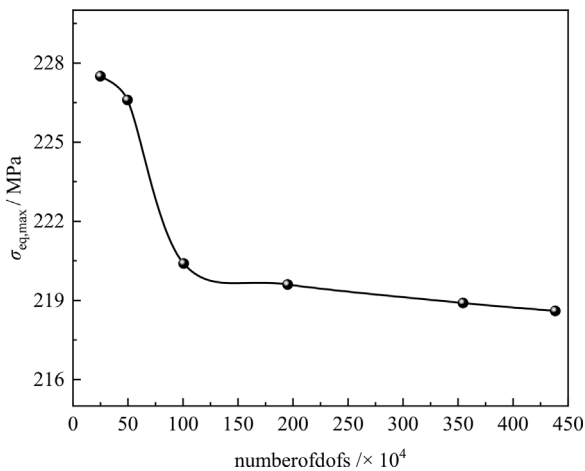


Fig. 5. Grid-independent analysis. The maximum equivalent stress of the tube produced by the $G = 2000 \text{ kg}/(\text{m}^2\text{s})$, $q_w = 150 \text{ kW}/\text{m}^2$ and $P = 25 \text{ MPa}$.

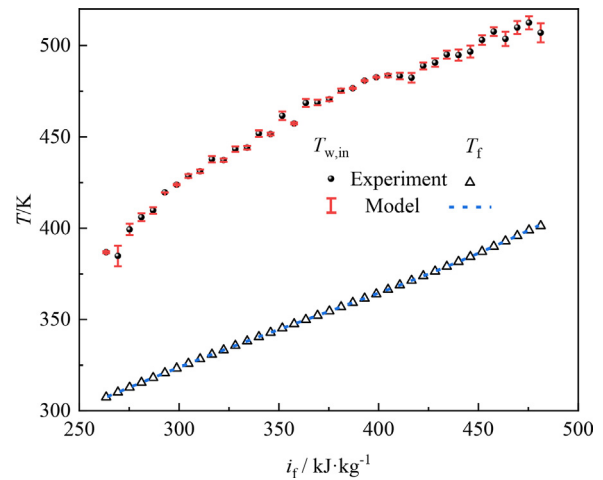


Fig. 6. Comparison of average temperature by experiment and simulation. The experiment results [13] of average fluid and wall temperature are shown by a triangle and black circle. The numerical results of these are shown by a blue dashed line and red arrow bar. The average deviation is employed to calculate the relative error.

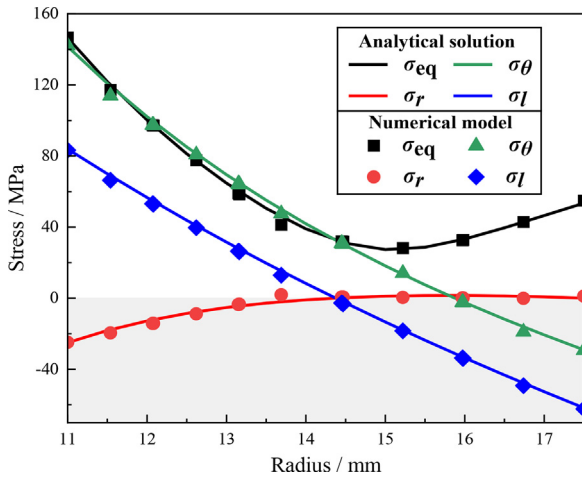


Fig. 7. Validation of structural model against theoretical solutions in three directions [31] and equivalent stress [32] produced by the $T_{w,i} = 792.4 \text{ K}$, $T_{w,o} = 827.5 \text{ K}$ and $P = 25 \text{ MPa}$.

tual working conditions. q_{max} is 150 kW/m^2 for the NUH case, and the total heat fluxes are the same for the three cases.

The temperature and stress profiles of the traditional tube under different heat fluxes are shown in Figs. 9–11. For the uniform heat flux (UH) case, the temperature and stress in the circumferential direction of the tube are distributed symmetrically. The variation of the circumferential temperature distribution of the NUH (Fig. 9(b)) is similar with the circumferential heat flux distribution (Fig. 4). The maximum temperatures for the NUH, HUH (half-cycle uniform heat flux) and the UH cases at $z = 0.5 \text{ m}$ were

873.5 K, 889.1 K and 833.7 K, respectively. The maximum equivalent stresses for the UH at $z = 0.5 \text{ m}$ was 140 MPa, occurred in the inner tube wall. Whereas, for the NUH and HUH, they were 172 MPa and 156 MPa, respectively, occurred in the outer tube wall at $\alpha = 180^\circ$, which were 22.9% and 11.4% higher compared to the UH case. As shown in Figs. 10 and 11, for the HUH and NUH conditions, the total stress consists of two components, and the thermal stress was much larger than the mechanical stress, which implied that the thermal stress dominated. Thus, effective methods or designs to reduce thermal stress should be investigated in subsequent studies.

3.2. A novel tube structure

The main characteristic of the NUH (Fig. 3) is that the heat flux on the rear side is low whereas the main heat flux acts on the heat-absorbing side (fireside). Thus, the heat resistance at the rear side slightly affects the heat absorption process, the heat intake of the tube is primarily at the fireside, and the heat resistance at the fireside significantly influences the heat transfer process. Therefore, the fireside should be optimized. Given that the tube thickness is proportional to the conduction thermal resistance, the tube thickness of the fireside should be reduced. The thermal resistance of the fireside should match the circumferential NUH distribution, i.e., it should be inversely distributed relative to the heat flux distribution (Fig. 3(c)).

Based on this principle, a novel structure tube is proposed to optimize the traditional tube, as shown in Fig. 12. First, the whole traditional tube was moved a distance of e (eccentric distance) toward the fireside, as shown in red Fig. 12(a). Next, the intersection of two tubes was taken to obtain the novel structure tube. Thus, the tube thickness distribution in the circumferential direction was

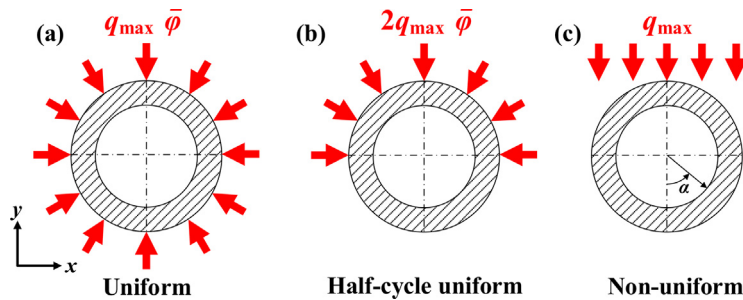


Fig. 8. Heat flux distribution. (a) Uniform case (b) Half-cycle uniform case (c) Non-uniform case. The total heat fluxes are the same for the three cases.

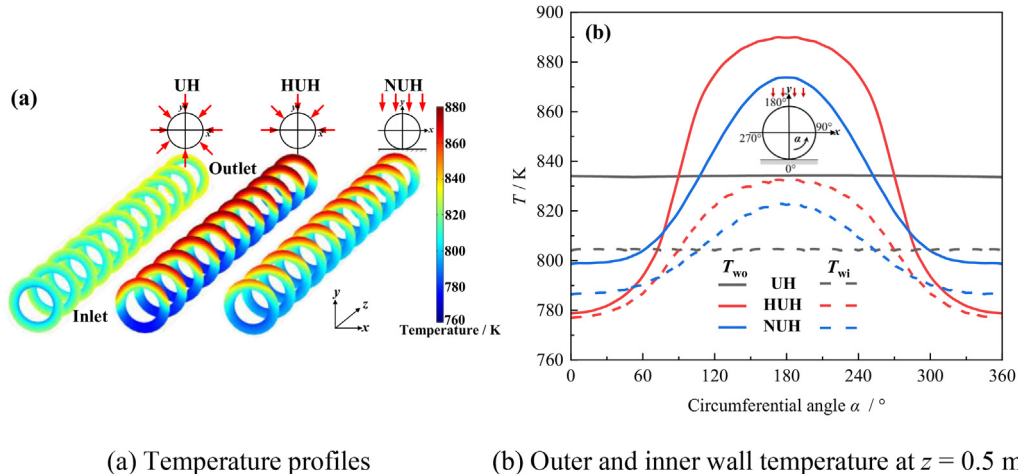


Fig. 9. Temperature distribution of traditional cooling wall tube for different heat fluxes. (a) Temperature profiles (b) Outer and inner wall temperature at $z = 0.5 \text{ m}$.

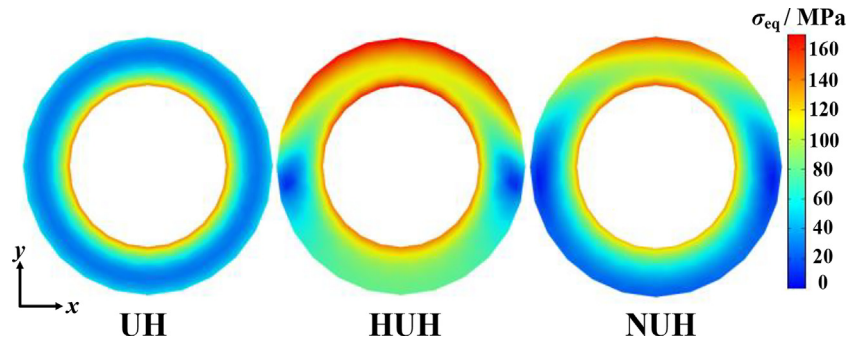


Fig. 10. Equivalent stress profiles of the tube for different heat fluxes at $z = 0.5$ m.

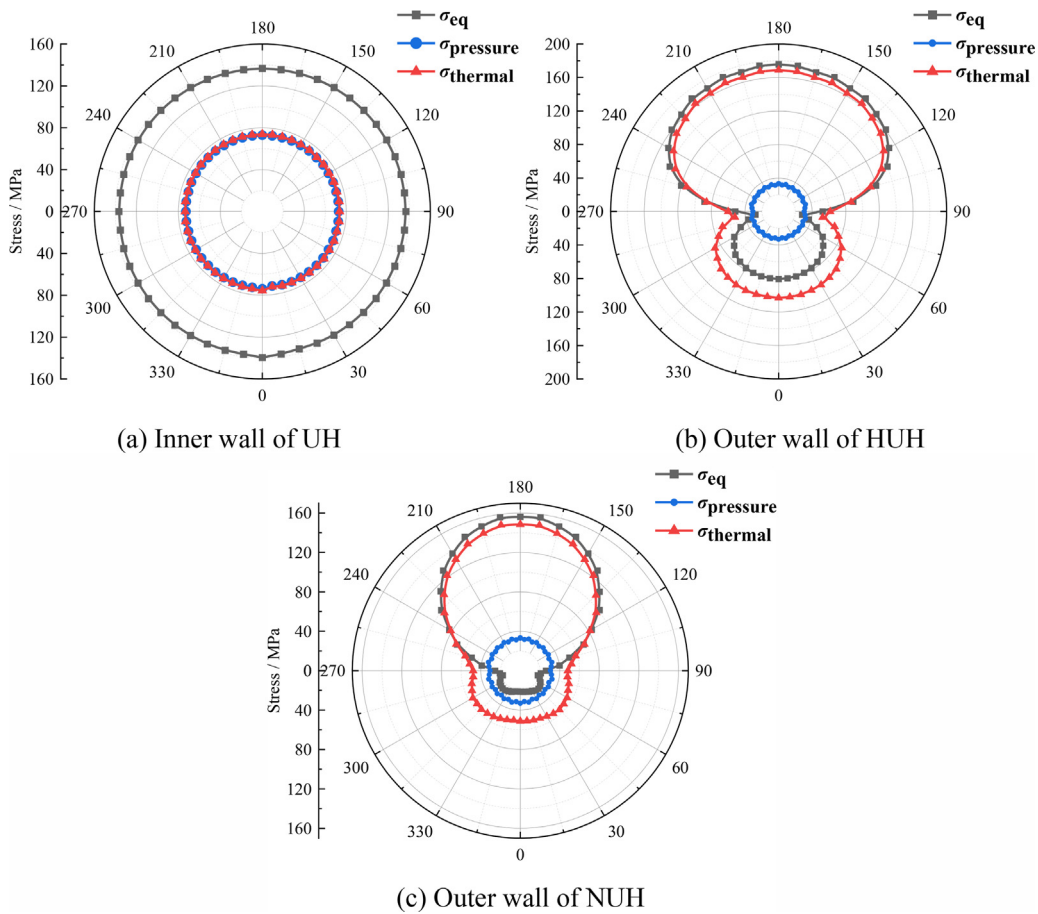


Fig. 11. Stress profiles of a traditional tube at $z = 0.5$ m. (a) Inner wall of UH (b) Outer wall of HUH (c) Outer wall of NUH.

changed. The tube thickness of the fireside decreased, and the tube thickness at the rear side did not change. These modifications allowed the low thermal conduction resistance to match the high heat flux, additionally, the tube material was also conserved.

In Fig. 12, it can be observed that, the wall thickness of the fire-side decreased with the increase of e , which is good for the heat transfer process, whereas, thinner wall thickness may cause safety problem. Hence, the minimum safe wall thickness (δ_m) [39] was considered, as expressed as follows:

$$\delta_m = \frac{PD}{2\sigma_{as}\xi + 2PY} \quad (1)$$

Where σ_{as} is the maximum allowable stress, ξ is the allowable stress correction factor, and Y is the correction coefficient.

The δ_m is a function of working parameters, such as tube material, working pressure, temperature, etc. The variation of δ_m of 316H with temperature is shown in Fig. 13. To ensure safety, δ_m increases with rising temperature, as σ_{as} follows the opposite trend. The δ_m increases 0.4 mm, when temperature changes from 773 K to 973 K. Thus, e is smaller at high temperature.

3.3. Comparison of traditional and novel tubes

The Eccentricity ($E_C = e / (R-r)$) was used to measure the unevenness of the wall thickness. A traditional tube has an Eccen-

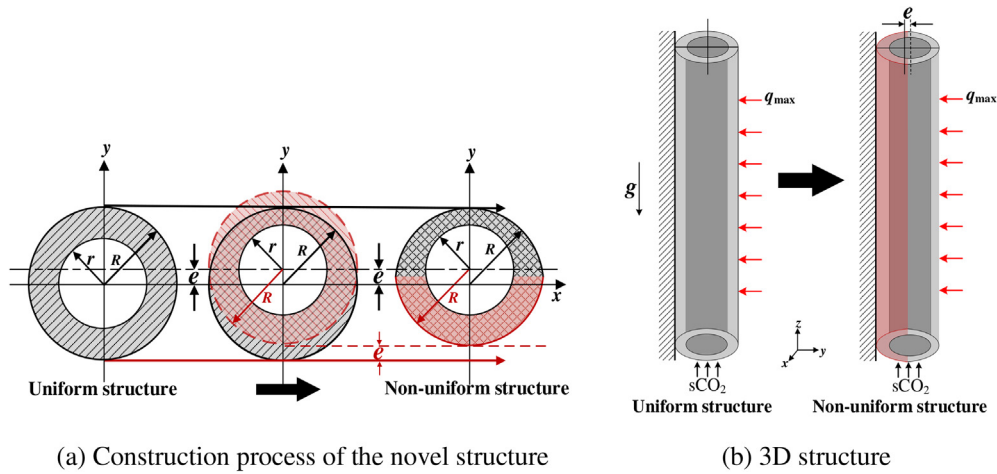


Fig. 12. Physical configuration of the proposed tube. (a) Construction process of the novel structure (b) 3D structure.

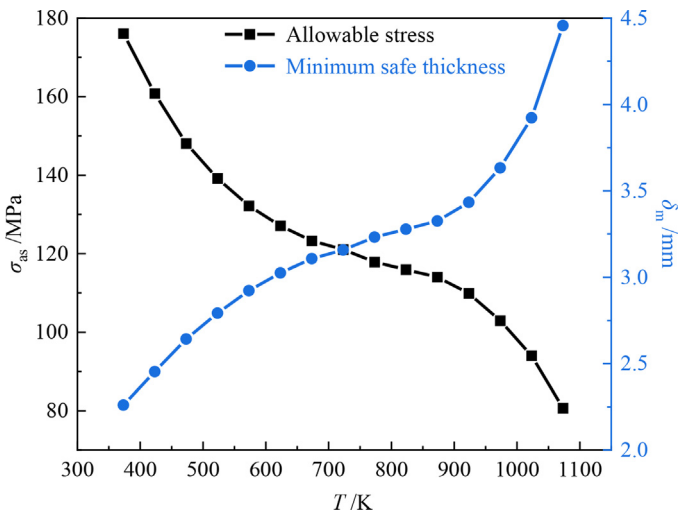


Fig. 13. σ_{as} and δ_m of 316H as a function of T .

tricity of 0. Traditional and proposed tubes are compared under different heat flux distributions in Figs. 14–16. The conditions are defined as follows: the sCO₂ inlet mass flux, q_{max} , and sCO₂ inlet temperature are 2000 kg/(m²s), 150 kW/m², and 773.15 K, respectively, and the working pressure is 25 MPa.

Fig. 14 shows the influences of E_c on the temperature difference ($\Delta T_w = |T_w - T_{ave}|$, in which T_{ave} is the cross-sectional average temperature) under different heat fluxes. For the UH case, ΔT_{wi} of the inner wall increased with the increase of E_c , indicating that the proposed structure is not applicable to the UH case. For the HUH case, ΔT_{wo} of the outer wall decreased with the increase of E_c . The maximum ΔT_{wo} at $z = 0.5$ m decreased from 71 to 47 K (approximately 33.8%), when E_c increased from 0 to 0.4. The variations of ΔT_{wo} under NUH were similar to those under HUH, whereas the reduction of ΔT_{wo} was smaller. The maximum ΔT_{wo} decreased from 58.5 to 41.5 K (approximately 29.1%), when E_c increased from 0 to 0.4. Additionally, comparing Figs. 14 and 11, it is observed that the thermal stress distribution is proportional to the temperature difference. Furthermore, the significant temperature difference induced by NUH and HUH resulted in severe thermal stress.

The thermal deviation factor (TDF) [24,40] had been proved to be another accurate and convenient criterion in the evaluation of

thermal stress under different working conditions. It was defined as follows:

$$TDF = \frac{|T - T_{ave}|}{T_s} \quad (2)$$

$$T_s = \frac{\sigma_s}{\alpha E} \quad (3)$$

where σ_s is yield strength.

Therefore, the TDF was also used to evaluate the stress in the non-uniform heating tubes. It was observed in Fig. 15 that the variation of TDF was similar with ΔT_w . For the UH case, TDF increased with the increase of E_c . For the HUH and NUH cases, TDF decreased with the increase of E_c . The maximum TDF at $z = 0.5$ m decreased from 1.75 to 1.19 (approximately 32%) for the HUH and 1.44 to 1 (approximately 30.6%) for the NUH, respectively, when E_c increased from 0 to 0.4. It further proved the proposed tube can effectively reduce thermal stress for HUH and NUH cases.

Fig. 16 shows that the pressure drops (ΔP) of the tubes was negligible for changes of E_c in all cases. The pressure drop was not affected by the Eccentricity. The maximum cross-sectional thermal stress ($\sigma_{t,max}$) decreased with the increase of E_c for both HUH and NUH conditions. Moreover, $\sigma_{t,max}$ decreased by 23 and 29% for HUH and NUH cases, respectively. In contrast, $\sigma_{t,max}$ increased by 7.8% for the UH condition.

As shown in Fig. 17, the maximum temperature of the tube wall decreased with increasing E_c . When E_c increased from 0 to 0.4, T_{max} decreased by 29.6 (3.3%) and 24.8 K (2.8%) for the HUH and NUH cases, respectively. Whereas T_{max} increased by 3 K (0.35%) for the UH condition. The novel structure can optimize the HUH and NUH conditions, however, the proposed structure is not applicable to the UH case.

To further validate the advantages of the novel structure, the proposed structure, traditional, and thin-walled tubes were compared (Figs. 18–20), where thickness of the thin-walled tube was equal to the thickness at $\alpha = 180^\circ$ of the proposed tube. The typical conditions are defined as follows: the sCO₂ inlet mass flux and sCO₂ inlet temperature are 2000 kg/(m²s) and 773.15 K, respectively, and the working pressure is 25 MPa. q_{max} of the novel structure was 150 kW/m², and the total heat flux of the traditional tube and thin-walled tube was equivalent to that of the proposed tube.

Fig. 19 shows the distribution of the cross-sectional temperature difference ($\Delta T = T_{max} - T_{min}$) and $\sigma_{eq,max}$ along the flow direction. ΔT of the traditional and thin-walled tubes was similar, which was approximately 24 K higher than that of the proposed

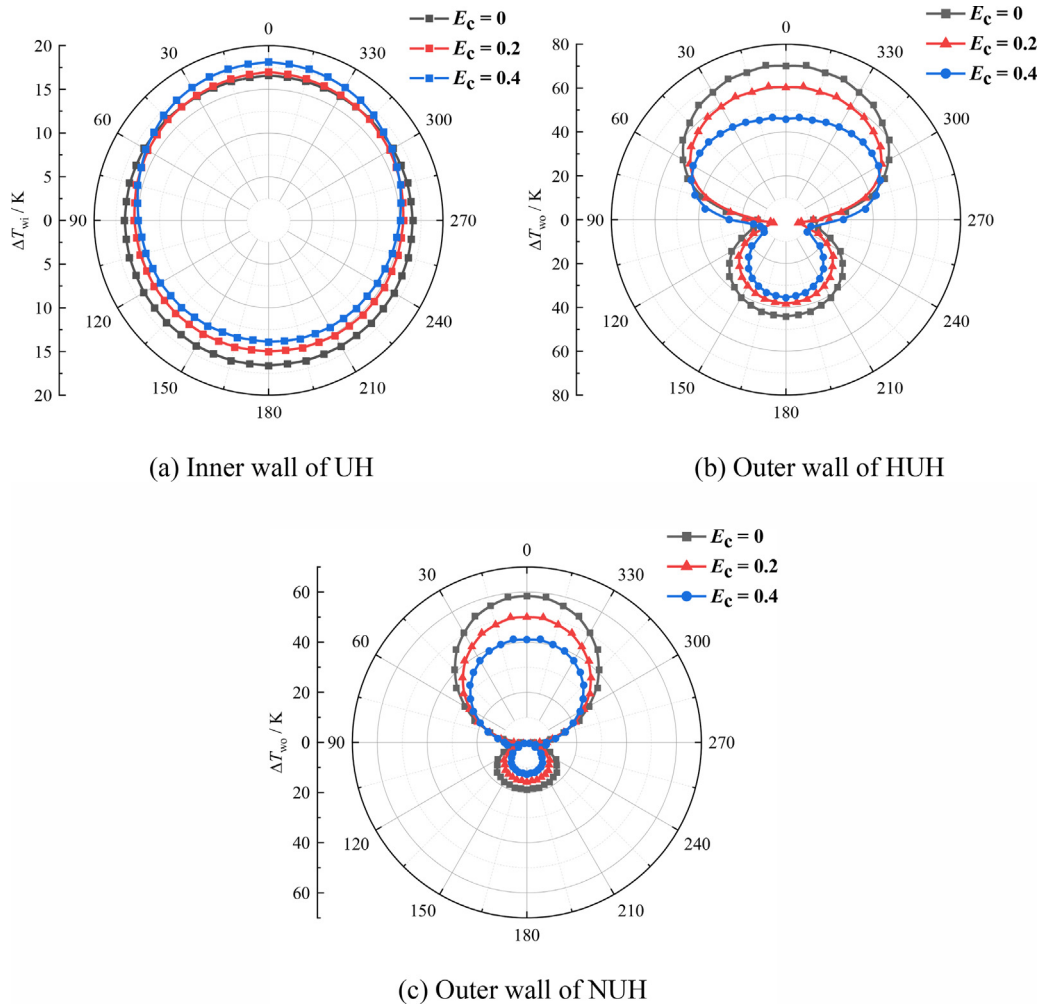


Fig. 14. ΔT_w profiles under different heat fluxes at $z = 0.5$ m. (a) Inner wall of UH (b) Outer wall of HUH (c) Outer wall of NUH.

tube. The $\sigma_{eq,max}$ of the thin-walled tube was the highest, whereas $\sigma_{eq,max}$ of the proposed tube was the smallest, which was 53 MPa and 71 MPa lower than that of the traditional tube and thin-walled tube, respectively. Furthermore, the maximum thermal stress at $z = 0.5$ m was effectively reduced in the proposed tube, which was approximately 43 MPa lower than that of the other two tubes, as shown in Fig. 20(a). It can be seen from Fig. 20(b) that the wall thickness at the fireside of novel structural tube was reduced but the equivalent stress of it was lower than that of the traditional tube and thin-walled tube. Thus, the optimization of a traditional tube under high NUH cannot be achieved by simply reducing the wall thickness. However, superior optimization is achieved using the proposed tube structure.

4. Conclusions

The maximum temperature and temperature difference are closely related to tube life span and economics. Lower maximum temperature and temperature difference result in better tube performance. In this study, a novel structure tube is proposed to improve its thermal-structural performance, and a three-dimensional thermal-fluid-mechanical coupling model was developed. The distributions of temperature, pressure drop, and stress of cooling wall tubes are numerically obtained. The effects of heat flux distribu-

tions on heat transfer performance were discussed. The conclusions are summarized below.

- (1) A novel structure tube is proposed by optimizing the coupling between circumferential heat flux and tube thickness on the heat-absorbing side to improve its comprehensive performance. The proposed structure will improve the safety and save tube material.
- (2) The proposed structure can optimize the half-cycle uniform and non-uniform heat flux conditions, however, it is not applicable to uniform heat flux condition. The thermal deviation factor and maximum temperature decrease with the increase of Eccentricity for both the half-cycle uniform and non-uniform heat flux conditions. The thermal deviation factor decreases by 32% and 30.6% and the maximum temperature decreases by 29.6 K (3.3%) and 24.8 K (2.8%) under the half-cycle uniform and non-uniform heat flux, respectively, when Eccentricity increases from 0 to 0.4.
- (3) The proposed structure, thin-walled tube, and traditional tube are compared, and results show that the performance of the proposed tube is the best. The maximum temperature decreases by approximately 55 K compared to a traditional and thin-walled tube. The maximum equivalent stress of the proposed tube is the smallest, which was 53 MPa and 71 MPa lower than that of the traditional tube and thin-walled tube, respectively.

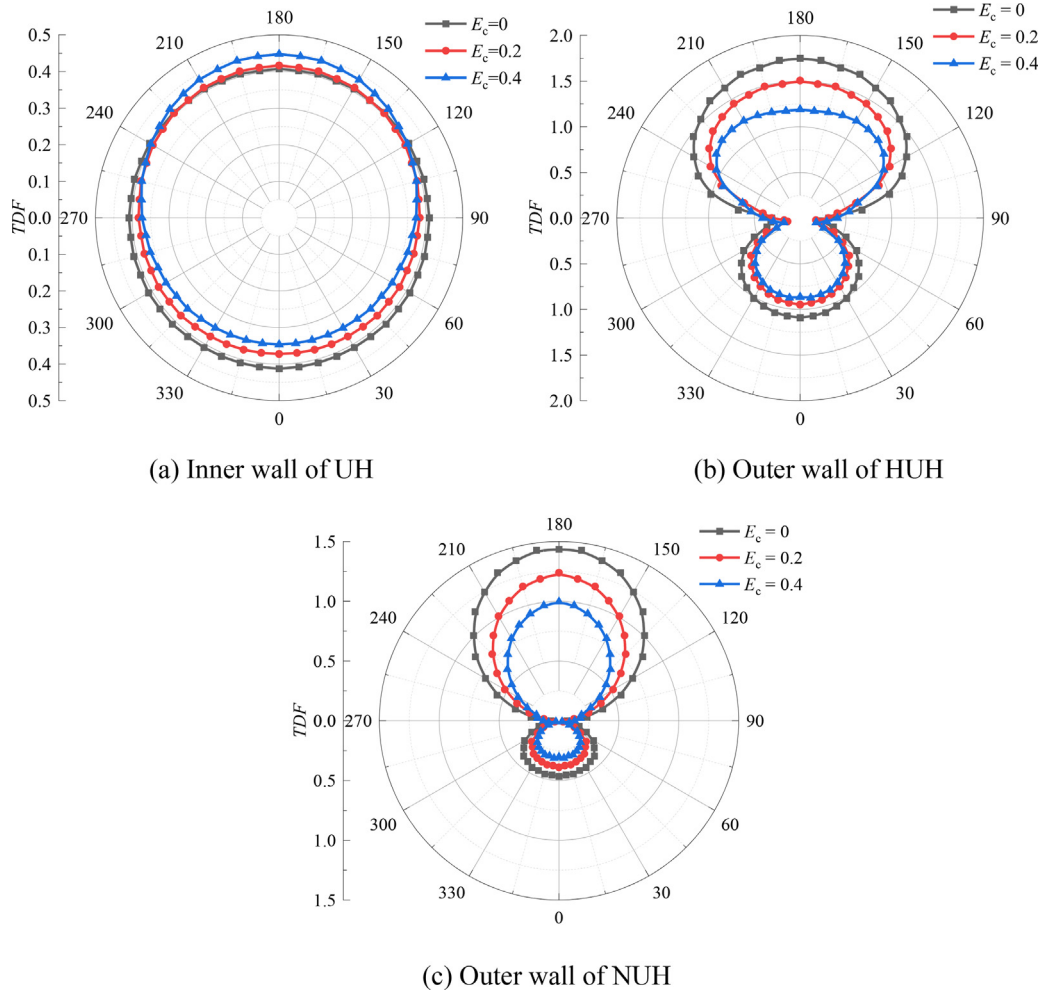


Fig. 15. TDF profiles for different heat fluxes at $z = 0.5$ m. (a) Inner wall of UH (b) Outer wall of HUH (c) Outer wall of NUH.

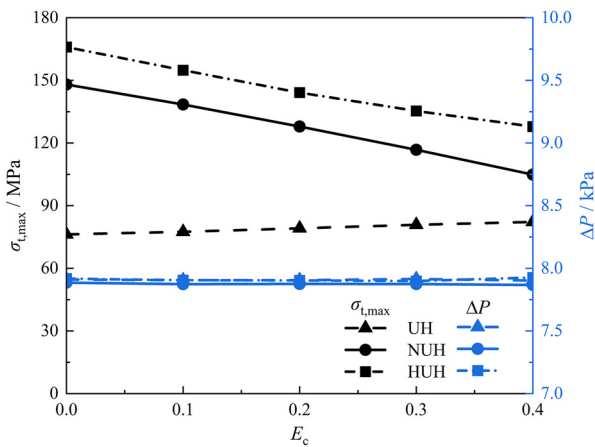


Fig. 16. Influence of E_c on $\sigma_{t,max}$ and ΔP .

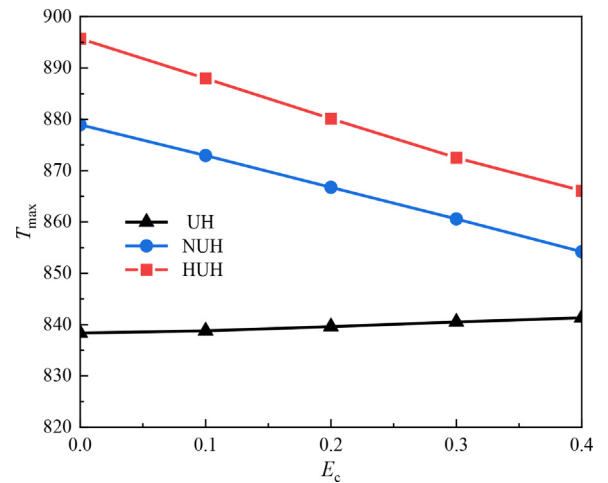


Fig. 17. Influence of E_c on the maximum temperature.

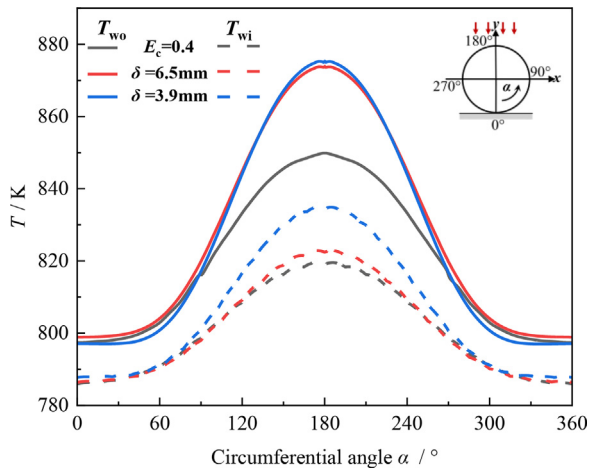


Fig. 18. Temperature profiles of the outer and inner surfaces at $z = 0.5$ m. The temperature of the proposed tube, traditional tube, and thin-walled tubes are shown in a black, red and blue line, respectively.

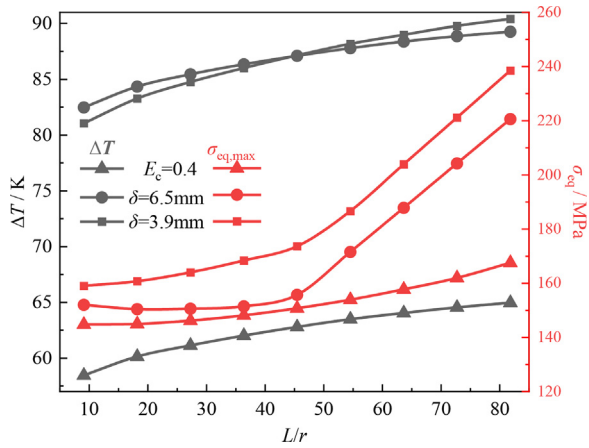


Fig. 19. Distribution of ΔT and $\sigma_{eq,max}$ along the flow direction.

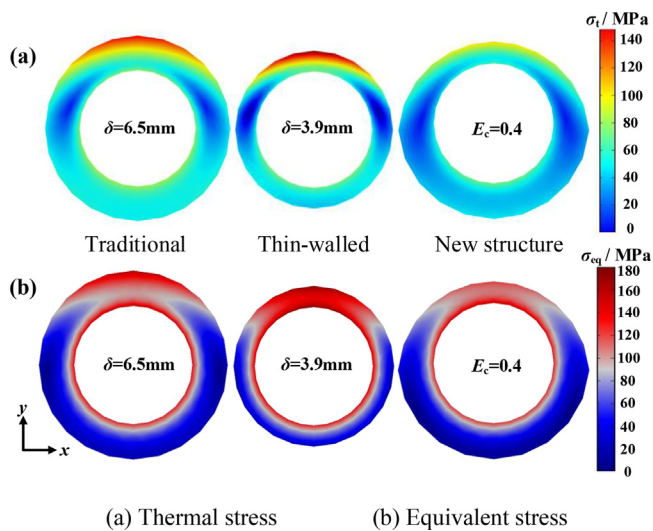


Fig. 20. Stress profiles of traditional, thin-walled and novel structure tube at $z = 0.5$ m. (a) Thermal stress (b) Equivalent stress.

Declaration of Competing Interest

The authors declare that they have no known competing financial interests or personal relationships that could have appeared to influence the work reported in this paper.

CRediT authorship contribution statement

Yan Juan Wang: Conceptualization, Methodology, Writing – original draft, Software. **Shuo Gao:** Data curation, Visualization, Validation, Investigation. **Wei Jie Shi:** Data curation, Formal analysis. **Qi Bin Liu:** Supervision, Writing – review & editing. **Jin Liang Xu:** Validation, Supervision.

Data availability

No data was used for the research described in the article.

Acknowledgments

The authors appreciate the financial support provided by the National Natural Science Foundation of China (Grant Nos. 52076075 and 52130608).

References

- [1] G.L. Liao, L.J. Liu, J.Q. E, F. Zhang, J.W. Chen, Y.W. Deng, H. Zhu, Effects of technical progress on performance and application of supercritical carbon dioxide power cycle: a review, *Energy Convers. Manag.* 199 (2019) 111986.
- [2] J.H. Park, H.S. Park, J.G. Kwon, T.H. Kim, M.H. Kim, Optimization and thermodynamic analysis of supercritical CO₂ Brayton recompression cycle for various small modular reactors, *Energy* 160 (2018) 520–535.
- [3] M. Mehrpooya, P. Bahramian, F. Pourfayaz, M.A. Rosen, Introducing and analysis of a hybrid molten carbonate fuel cell-supercritical carbon dioxide Brayton cycle system, *Sustain. Energy Technol. Assess.* 18 (2016) 100–106.
- [4] J.L. Xu, X. Wang, E.H. Sun, M.J. Li, Economic comparison between sCO₂ power cycle and water-steam Rankine cycle for coal-fired power generation system, *Energy Convers. Manag.* 238 (2021) 114150.
- [5] Y.H. Fan, G.H. Tang, X.L. Li, D.L. Yang, General and unique issues at multiple supercritical carbon dioxide power system: a review on recent advances, *Energy Convers. Manag.* 268 (2022) 115993.
- [6] D. Fleming, T. Holschuh, T. Conboy, G. Rochau, R. Fuller, Scaling Considerations for a Multi-Megawatt Class Supercritical CO₂ Brayton Cycle and Path Forward for Commercialization, in: *ASME Turbo Expo 2012: Turbine Technical Conference and Exposition*, 2012, pp. 953–960.
- [7] J.Q. Guo, K. Wang, H.H. Zhu, Y.L. He, Thermodynamic analysis of brayton cycles using supercritical carbon dioxide and its mixture as working fluid, *J. Eng. Thermophys.* 38 (04) (2017) 695–702.
- [8] R.C. Qiu, Simulation Study on Solar Power Tower System Based on Supercritical CO₂ Brayton Cycle. [D], Zhejiang University, 2018.
- [9] A. Askarova, S. Bolegenova, V. Maximov, M. Beketayeva, P. Safarik, Numerical modeling of pulverized coal combustion at thermal power plant boilers, *J. Therm. Sci.* 24 (3) (2015) 275–282.
- [10] Y.J. Wang, B.H. Yu, S. Gao, Q.B. Liu, J.L. Xu, Performance analysis of cooling wall of supercritical CO₂ coal-fired plants, *J. Therm. Sci.* 31 (6) (2022) 1881–1890.
- [11] K. Wang, X.Y. Zhang, Z.D. Zhang, C.H. Min, Three-dimensional shape optimization of fins in a printed circuit recuperator using S-CO₂ as the heat-transfer fluid, *Int. J. Heat Mass Transf.* 192 (2022) 122910.
- [12] K. Brun, P. Friedman, R. Dennis, *Fundamentals and Applications of Supercritical Carbon Dioxide (sCO₂) Based Power Cycles*, Woodhead publishing, 2017.
- [13] B.G. Zhu, J.L. Xu, X.M. Wu, J. Xie, M.J. Li, Supercritical “boiling” number, a new parameter to distinguish two regimes of carbon dioxide heat transfer in tubes, *Int. J. Therm. Sci.* 136 (2019) 254–266.
- [14] H.Z. Li, Y.F. Zhang, M.Y. Yao, Y. Yang, W.L. Han, W.G. Bai, Design assessment of a 5 MW fossil-fired supercritical CO₂ power cycle pilot loop, *Energy* 174 (2019) 792–804.
- [15] C. Liu, J.L. Xu, M.J. Li, Q.Y. Wang, G.L. Liu, The comprehensive solution to decrease cooling wall temperatures of sCO₂ boiler for coal fired power plant, *Energy* 252 (2022) 124021.
- [16] J. Zhou, M. Zhu, K. Xu, S. Su, Y.F. Tang, S. Hu, Y. Wang, J. Xu, L.M. He, J. Xiang, Key issues and innovative double-tangential circular boiler configurations for the 1000 MW coal-fired supercritical carbon dioxide power plant, *Energy* 199 (2020) 117474.
- [17] D.L. Yang, G.H. Tang, Y.H. Fan, X.L. Li, S.Q. Wang, Arrangement and three-dimensional analysis of cooling wall in 1000 MW S-CO₂ coal-fired boiler, *Energy* 197 (2020) 117168.
- [18] C. Liu, J.L. Xu, G.H. Liu, Layout and optimization of heat-transfer surfaces in boilers for coal-fired supercritical CO₂ power system (in Chinese), *Sci. SINTECH* 51 (2021) 1507–1518, doi:10.1360/SST-2021-0062.

- [19] H.Q. Chu, N. Xu, X.Y. Yu, H.T. Jiang, W.G. Ma, F. Qiao, Review of surface modification in pool boiling application: coating manufacturing process and heat transfer enhancement mechanism, *Appl. Therm. Eng.* 215 (2022) 119041.
- [20] H.Q. Chu, X.Y. Yu, H.T. Jiang, D.D. Wang, N. Xu, Progress in enhanced pool boiling heat transfer on macro-and micro-structured surfaces, *Int. J. Heat Mass Transf.* 200 (2023) 123530.
- [21] Y.L. He, K. Wang, B.C. Du, Y. Qiu, Z.J. Zheng, Q. Liang, Non-uniform characteristics of solar flux distribution in the concentrating solar power systems and its corresponding solutions: a review, (2016). https://scholar.google.com/scholar?hl=zh-CN&as_sdt=0%2C5&q=Non-uniform+characteristics+of+solar+flux+distribution+in+the+concentrating+solar+power+systems+and+its+corresponding+solutions%3A+A+review&btnG=.
- [22] J.M. Christian, J.D. Ortega, C.K. Ho, J. Yellowhair, ASME, design and modeling of light-trapping tubular receiver panels, in: Proceedings of the 10th ASME International Conference on Energy Sustainability, Charlotte, NC, 2016.
- [23] Y. Liu, Y. Dong, L.T. Xie, Zhang C.Z, C. Xu, Heat transfer enhancement of supercritical CO₂ in solar tower receiver by the field synergy principle, *Appl. Therm. Eng.* 212 (2022) 118479.
- [24] X.L. Li, G.H. Tang, D.L. Yang, Y.H. Fan, J.L. Xu, Thermal-hydraulic-structural evaluation of S-CO₂ cooling wall tubes: a thermal stress evaluating criterion and optimization, *Int. J. Therm. Sci.* 170 (2021) 107161.
- [25] X.L. Li, G.H. Tang, Y.H. Fan, D.L. Yang, A performance recovery coefficient for thermal-hydraulic evaluation of recuperator in supercritical carbon dioxide Brayton cycle, *Energy Convers. Manag.* 256 (2022) 115393.
- [26] B.C. Du, Y.L. He, Z.J. Zheng, Z.D. Cheng, Analysis of thermal stress and fatigue fracture for the solar tower molten salt receiver, *Appl. Therm. Eng.* 99 (2016) 741–750.
- [27] E.W. Lemmon, M.L. Huber, M.O. McLinden, 2010. NIST standard reference database 23, reference fluid thermodynamic and transport properties (REFPROP), version 9.0, National institute of standards and technology. File dated December 22: 2010. https://www.nist.gov/system/files/documents/srd/REFPROP8_manua3.htm.
- [28] Y.J. Wang, Q.B. Liu, J. Lei, H.G. Jin, Performance analysis of a parabolic trough solar collector with non-uniform solar flux conditions, *Int. J. Heat Mass Transf.* 82 (2015) 236–249.
- [29] F.R. Menter, Two-equation eddy-viscosity turbulence models for engineering applications, *AIAA J.* 32 (8) (1994) 1598–1605.
- [30] W.P. Jones, B.E. Launder, The prediction of laminarization with a two-equation model of turbulence, *Int. J. Heat Mass Transf.* 15 (2) (1972) 301–314.
- [31] T.W. Neises, M.J. Wagner, A.K. Gray, ASME, structural design considerations for tubular power tower receivers operating at 650 °C, in: Proceedings of the ASME 8th International Conference on Energy Sustainability, Boston, MA, Seaport World Trade Ctr, 2014.
- [32] K. Wang, P.S. Jia, Y. Zhang, Z.D. Zhang, T. Wang, C.H. Min, Thermal-fluid-mechanical analysis of tubular solar receiver panels using supercritical CO₂ as heat transfer fluid under non-uniform solar flux distribution, *Sol. Energy* 223 (2021) 72–86.
- [33] D.C. Wilcox, Turbulence Modeling For CFD, DCW industries La Canada, CA, 1998.
- [34] S.V. Patankar, Numerical Heat Transfer and Fluid Flow, CRC press, 2018.
- [35] E.H. Sun, J.L. Xu, M.J. Li, G.L. Liu, B.G. Zhu, Connected-top-bottom-cycle to cascade utilize flue gas heat for supercritical carbon dioxide coal fired power plant, *Energy Convers. Manag.* 172 (2018) 138–154.
- [36] P. Duda, J. Taler, A new method for identification of thermal boundary conditions in water-wall tubes of boiler furnaces, *Int. J. Heat Mass Transf.* 52 (5–6) (2009) 1517–1524.
- [37] J. Taler, P. Duda, B. Węglowski, W. Zima, S. Grądziel, T. Sobota, D. Taler, Identification of local heat flux to membrane water-walls in steam boilers, *Fuel* 88 (2) (2009) 305–311.
- [38] J.M. Wang, X. Chen, C. Zhang, M.Y. Gu, H.Q. Chu, Numerical investigation of heat transfer characteristics of supercritical CO₂ tube in combustion chamber of coal-fired boiler, *J. Therm. Sci.* 28 (3) (2019) 442–453.
- [39] J.D. Ortega, J.M. Christian, C.K. Ho, ASME, structural analysis of a direct heated tubular solar receiver for supercritical CO₂ Brayton cycle, in: Proceedings of the 9th ASME International Conference on Energy Sustainability, San Diego, CA, 2015.
- [40] X.L. Li, G.X. Li, G.H. Tang, Y.H. Fan, D.L. Yang, A generalized thermal deviation factor to evaluate the comprehensive stress of tubes under non-uniform heating, *Energy* 263 (2023) 125710.